Available online at www.sciencedirect.com
SCIENCE DIRECT®
ELSEVIER
Journal of Nuclear Materials 321 (2003) 305–312
journal of nuclear materials
www.elsevier.com/locate/jnucmat

The effect of irradiation-induced gas-atom re-solution on grain-boundary bubble growth ☆

J. Rest

Argonne National Laboratory, Energy Technology-212, 9700 S. Cass Avenue, Argonne, IL 60439-4815, USA

Received 26 December 2002; accepted 3 June 2003

Abstract

The rim region of high-burnup fuels is characterized by an exponential growth of intergranular porosity. In particular, the understanding of the dynamics of irradiation-induced recrystallization and subsequent gas-bubble swelling requires a quantitative assessment of the nucleation and growth of grain-boundary bubbles. Calculations of bubble growth on the grain boundaries of irradiated nuclear fuels at relatively low temperatures have, in general, been performed under the assumption that these bubbles are not appreciably affected by irradiation-induced gas-atom re-solution. In contrast, matrix bubbles are strongly affected by this bubble shrinkage mechanism and as a consequence are generally two to three orders or more of magnitude smaller than the grain-boundary bubbles. A variational method is used to calculate diffusion from a spherical fuel grain. The junction position of two trial functions is set equal to the bubble gas-atom knock out distance. The effect of grain size, gas-atom re-solution rate and diffusivity, gas-atom knock out distance, and grain-boundary bubble density on the growth of intergranular bubbles is studied, and the conditions under which intergranular bubble growth occurs are elucidated.

1. Introduction

After a short period of irradiation, the intragranular structure of UO_2 is populated with a high-density ($\approx 10^{23}$ m^{-3}) of small ($r \approx 10^{-9}$ m) bubbles [1], separated by ≈5–10 bubble diameters. In general, observations that bubbles confined to the bulk (lattice) material of irradiated nuclear fuels do not grow to appreciable sizes at low temperatures (fuel temperatures where the gas-atom diffusivity is irradiation enhanced, i.e. <0.5 melting temperature) are ascribed to the effect of irradiation-induced re-solution [2,3]. Gas-atom re-solution is a dynamic bubble shrinkage mechanism wherein fission fragments either directly or indirectly cause gas atoms to be lost from a bubble. Only when sinks, such as grain boundaries, are present in the material can bubbles grow to sizes observable with a scanning electron microscope [4]. Most calculations on intergranular gas behavior found in the literature have focused on the condition for grain-face saturation and have not addressed the specific mechanics of intergranular bubble growth in the presence of irradiation-induced re-solution [5–8]. This author has performed calculations of grain-boundary bubble growth under the assumption that the effective gas-atom re-solution rate from grain-boundary bubbles is negligible [9–11]. This assumption has relied on heuristic arguments [12] that the strong sink-like nature of a grain boundary provides a relatively short recapture distance for gas that has been knocked out of a bubble, and as such neutralizes the 'shrinking' effect of the re-solution process. These grain-boundary bubbles grow at an enhanced rate as compared to those in the bulk material. The importance of understanding the physics underlying intergranular bubble growth is underscored by the rim region of high-burnup fuels which are

☆ Work supported by the US Department of Energy, Office of Arms Control and Nonproliferation, under contract W-31-109-Eng-38.

E-mail address: jrest@anl.gov (J. Rest).

0022-3115/$ - see front matter © 2003 Elsevier B.V. All rights reserved.
doi:10.1016/S0022-3115(03)00303-9

characterized by an exponential growth of intergranular porosity towards the pellet edge: a narrow band of fully recrystallized porous material exists at the pellet periphery, and a rather wide adjacent transition zone with partially recrystallized porous areas appears dispersed within the original matrix structure [13]. In particular, the understanding of the dynamics of irradiation-induced recrystallization and subsequent gas-bubble swelling requires a quantitative assessment of the nucleation and growth of grain-boundary bubbles [11,13].

The purpose of this paper is to present a mechanistic model for the growth of grain-boundary bubbles during irradiation at relatively low temperatures (i.e. where gas-atom diffusion is athermal) and, thus, to quantify the effect of gas-atom re-solution on their growth. A variational method is used to calculate diffusion from a spherical fuel grain. The junction position of two trial functions is set equal to the bubble gas-atom knock out distance. The effect of grain size, gas-atom re-solution rate and diffusivity, gas-atom knock out distance, and grain-boundary bubble density on the growth of intergranular bubbles is studied, and the conditions under which intergranular bubble growth occurs are elucidated.

2. Flux algorithm

The flux of gas atoms diffusing to the grain boundaries in a concentration gradient is obtained by solving for the concentration of gas atoms C_g within a spherical grain that satisfies the equation

$$\frac{\partial C_g}{\partial t} = \frac{1}{r^2}\frac{\partial}{\partial r}\left(D_g r^2 \frac{\partial C_g}{\partial r}\right) + \alpha \overset{*}{f} + \overset{*}{f}(\lambda)_{\text{boundary}}, \tag{1a}$$

where D_g is the gas-atom diffusion coefficient, $\overset{*}{f}$ is the fission rate, α is the average number of rare-gas atoms produced per fission, and r is the radial distance from the grain center, and $\overset{*}{f}(\lambda)_{\text{boundary}}$ is the flux of gas atoms from the boundary bubbles due to irradiation-induced re-solution. This back flux of gas can be thought of as an additional matrix gas-atom generation mechanism and is assumed to be distributed uniformly within a spherical annulus of thickness λ, where λ is the gas-atom knock out distance. In Eq. (1), intragranular bubble trapping of fission gas has been neglected. However, this effect can be modeled by using an effective diffusion coefficient given by [12]

$$D_g^{\text{eff}} = \frac{b}{b+g} D_g, \tag{1b}$$

where b is the gas-atom re-solution rate and g is the probability per second of a gas atom in solution being captured by an intragranular bubble. Observed concentrations $\approx 10^{23}$ m^{-3} of intragranular bubbles of ≈ 1 nm radius [12] with $b = 2 \times 10^{-4}$ s^{-1} yields a value for $g = 2.5 \times 10^{-4}$ s^{-1} and $D_g^{\text{eff}} = 0.44 D_g$.

In general, Eq. (1a) is solved with the boundary conditions

$$C_g = 0 \quad \text{at } t = 0 \quad \text{for} \quad 0 \leqslant r \leqslant d_g/2, \tag{2a}$$

$$C_g = 0 \quad \text{at } r = d_g/2 \quad \text{for} \quad t_0 \leqslant t \leqslant t_0 + \delta t, \tag{2b}$$

$$\frac{\partial C_g}{\partial r} = 0 \quad \text{at } r = 0 \quad \text{for} \quad t_0 \leqslant t \leqslant t_0 + \delta t, \tag{2c}$$

where δt is an increment of time and d_g is the grain diameter. For an increment of time δt the concentration of gas atoms in a spherical grain described in Eq. (1a) is

$$\frac{1}{r^2}\frac{\mathrm{d}}{\mathrm{d}r}\left(D_g r^2 \frac{\mathrm{d}C_g}{\mathrm{d}r}\right) - \frac{C_g}{\delta t} + \frac{C_g^0}{\delta t} + \alpha \overset{*}{f} + \overset{*}{f}(\lambda)_{\text{boundary}} = 0. \tag{3}$$

Euler's theorem may now be used to obtain a variational principle equivalent to Eq. (3):

$$\delta \int_0^{1/2d_g} 4\pi \left[\frac{D_g}{2}\left(\frac{\mathrm{d}C_g}{\mathrm{d}r}\right)^2 + \frac{C_g^2}{2\,\delta t} - \left(\frac{C_g^0}{\delta t} + \alpha \overset{*}{f} + \overset{*}{f}(\lambda)_{\text{boundary}}\right) C_g\right] r^2 \,\mathrm{d}r = 0, \tag{4}$$

which assumes that Dirichlet boundary conditions are to be applied. An approximate solution to the problem may now be obtained by choosing a trial function that satisfies the boundary conditions and minimizes the integral in Eq. (4) in terms of free parameters in the function. Many types of trial function could be chosen, but it is easier to work with piecewise functions than global functions. Quadratic functions are attractive because they allow an exact representation of Eq. (1a) for long times. Matthews and Wood [14] obtained a realistic level of accuracy with a minimum of computer storage and running time by splitting the spherical grain into two concentric regions of approximately equal volume. In each region, the gas concentration was represented by a quadratic function. In the inner region the concentration function was constrained to have $\mathrm{d}C_g/\mathrm{d}r = 0$ at $r = 0$. In the outer region, the concentration function was constrained to a value of $C_g = 0$ at $r = d_g/2$. The two functions were also constrained to be continuous at the common boundary of the two regions. This left three free parameters: the concentrations C_1^g, C_2^g, and C_3^g, respectively, for the radius ratio $\rho_1 = 0.2$, $\rho_2 = 0.4$, and $\rho_3 = 0.45$, where $\rho = r/d_g$. These positions are the midpoint radii of the inner region, the boundary between the regions, and the midpoint radius of the outer region, respectively.

However, this method is too crude if one is interested in an accurate representation of the concentration gradient in the presence of irradiation-induced re-solution from grain-boundary bubbles where the gas-atom knock out distance λ is on the order of 100 Å [15]. In this case it is necessary to formulate the problem in terms of λ. The radius ratio at the interface of the two regions is now expressed as

$$\rho_\lambda = 1/2 - \lambda/d_g. \tag{5}$$

The trial functions are as follows:

For the inner region,

$$C_g(\rho) = 4[C_1^g(\rho_\lambda^2 - \rho^2) + C_2^g(\rho^2 - \rho_\lambda^2/4)]/3\rho_\lambda^3. \tag{6}$$

For the outer region,

$$C_g(\rho) = \frac{C_2^g}{(2\rho_\lambda - 1)^2}[8\rho^2 - 2(2\rho_\lambda + 3)\rho + 2\rho_\lambda + 1] + \frac{8C_3^g}{(2\rho_\lambda - 1)^2}[(2\rho_\lambda + 1)\rho - 2\rho^2 - \rho_\lambda]. \tag{7}$$

Eqs. (6) and (7) are substituted for C_g in Eq. (4) and an extremum is found by differentiating with respect to C_1^g, C_2^g, and C_3^g. This results in a set of three coupled algebraic equations that can be directly solved to obtain the concentrations C_1^g, C_2^g, and C_3^g, as follows:

$$C_1^g = \frac{X_1 - F_2 C_2^g}{F_1}, \tag{8}$$

$$C_2^g = \frac{\frac{F_2}{F_1}X_1 + \frac{F_4}{F_5}X_3 - X_2}{\frac{F_2}{F_1}F_2 + \frac{F_4}{F_5}F_4 - F_3}, \tag{9}$$

and

$$C_3^g = (X_3 - F_4 C_2^g)/F_5, \tag{10}$$

where

$$\begin{aligned} F_1 &= q_1 D_g \delta t/d_g^2 + q_2, \\ F_2 &= q_3 D_g \delta t/d_g^2 + q_4, \\ F_3 &= q_5 D_g \delta t/d_g^2 + q_6, \\ F_4 &= q_7 D_g \delta t/d_g^2 + q_8, \\ F_5 &= q_9 D_g \delta t/d_g^2 + q_{10}, \end{aligned} \tag{11}$$

and

$$\begin{aligned} X_1 &= \overset{*}{\alpha f}\,\delta t q_{11} + C_1^0 q_2 + C_2^0 q_4, \\ X_2 &= \overset{*}{\alpha f}\,\delta t q_{12} + C_1^0 q_4 + C_2^0 q_6 + C_3^0 q_8, \\ X_3 &= (\overset{*}{\alpha f} + \overset{*}{f}_{\text{boundary}})\,\delta t q_{13} + C_2^0 q_8 + C_3^0 q_{10}, \end{aligned} \tag{12}$$

where C_1^0, C_2^0, and C_3^0 are the values of the concentrations at the evaluation points at the start of the time increment. The various q coefficients are integrals that depend on ρ and are given in Appendix A.

The flux of gas atoms to the boundary (in units of atoms/m^3/s) is given by

$$J = -\frac{4D_g}{d_g}\frac{\partial C}{\partial \rho}\bigg|_{\rho=1/2}, \tag{13}$$

or

$$J = \frac{4D_g}{d_g(1 - 2\rho_\lambda)}(4C_3^g - C_2^g). \tag{14}$$

When $\rho_\lambda = 0.4$ Eqs. (6), (7) and (14) reduce to those derived in Ref. [14] for the special case of fixed spatial nodes (Ref. [14] defines $\rho = 2r/d_g$. Thus $\rho \to \rho/2$ to convert from the present treatment to the one described in Ref. [14]). The variational method described above has been compared to finite difference calculations. Suitable choice of step length δ results in insignificant time-step sensitivity with comparable accuracy to the finite difference approach with one-fifth–one-tenth computer time [16].

3. Grain-boundary bubble growth

The bubble radius R_b is calculated using the Van der Waals equation of state, i.e.

$$\frac{2\gamma}{R_b}\left(\frac{4}{3}\pi R_b^3 - b_v n\right) = nkT, \tag{15}$$

where γ is the surface tension, T is the temperature in K, k is Boltzman's constant, b_v is the Van der Waals constant, and n is the number of gas atoms in a grain-boundary bubble, i.e.

$$n(t) = \sum_{\delta t}(f_c J(t)/N_b + z(1 - f_c)D_g C_g^b - bn(t))\,\delta t, \tag{16}$$

where b is the gas-atom re-solution rate (s^{-1}), $f_c \approx \pi r_b^2 N_b$ is the fractional coverage of the grain boundary by bubbles, z is a grain-boundary diffusion enhancement factor, N_b is the total number of bubbles on the boundary (bubbles/m^2), and C_g^b is the gas-atom concentration on grain boundaries (atoms/m^2), i.e.

$$C_g^b = \sum_{\delta t}\left((1 - f_c)J(t) - zD_g C_g^b N_b\right)\delta t. \tag{17}$$

When f_c is small (e.g., during the initial stages of boundary bubble growth) most of the gas reaching the boundary exists as single gas atoms and diffuses by random walk to the boundary bubbles. This is analogous to gas-atom accumulation by bubbles in the grain interior. When f_c is large, the majority of the gas

reaching the boundary flows directly into boundary bubbles. The grain-boundary enhancement factor, z, accounts for the general view that gas-atom diffusion on the boundary is more rapid than in the matrix due to the existence of more space and sites (e.g., ledges) from which and to which the gas atoms can hop.

In general, the gas-atom re-solution rate, b, is dependent on the damage rate and on the bubble size. b is calculated under the assumption that gas-atom re-solution from a spherical bubble is isotropic and proceeds by the ejection of single gas atoms. Thus,

$$b = \frac{3b_0\overset{*}{f}}{R_b}\int_{R_b-\lambda}^{R_b}\left(\frac{1+\cos\phi}{2}\right)r^2\,dr, \tag{18}$$

where b_0 is a constant and

$$\cos\phi = (R_b^2 - \lambda^2 - r^2)/2r\lambda. \tag{19}$$

Gas atoms that are knocked out of grain-boundary bubbles (the second term on the right-hand side of Eq. (16)) are evenly dispersed within an annulus of thickness λ adjacent to the grain boundary. This backward flux of gas atoms affects the concentration gradient of gas atoms from the matrix to the boundary, and thus the overall flux of gas atoms to the boundary. Thus, this backward flux of gas atoms, in atoms/m^2/s, can be thought of as an additional matrix gas-atom generation mechanism (last term on the right-hand side of Eq. (1a)) and is given by

$$\overset{*}{f}(\lambda)_{\text{boundary}} = \frac{3bN_b n(t)}{d_g}\frac{V}{V_\lambda}, \tag{20}$$

where V is the volume of the grain and V_λ is the volume of the annulus of thickness λ within which the backward flux of gas atoms from the boundary bubbles is deposited. In Eq. (20), the first ratio on the right-hand side represents the backward flux of gas (atoms/m^3/s) and the second ratio the fraction of the intragranular volume within which this gas is deposited. This value is independent of λ. Thus, as λ decreases V_λ becomes smaller and $\overset{*}{f}(\lambda)_{\text{boundary}}$ increases.

Finally, the fractional gas release to the grain boundary F is given by

$$F = \frac{3}{d_g\sum_{\delta t}\alpha\overset{*}{f}\,\delta t}\sum_{\delta t}(J(t) - bn(t)N_b)\,\delta t. \tag{21}$$

4. Analysis of bubble growth on grain boundaries

Bubble growth on grain boundaries will continue until a saturation condition is reached wherein the bubbles initiate contact with each other. Subsequently these bubbles link up and vent their gas to the grain edges where, once tunnels of open porosity form the gas is released to the fuel exterior [4]. The saturation condition is given by

$$f_c = \pi N_b^s R_b^2 \sin^2\theta_b = f_b, \tag{22}$$

where the bubbles are lenticular-shaped pores comprising spherical caps which are joined in the plane of the boundary with dihedral angle $2\theta = 100°$ [17], and f_b is the value of the fractional coverage of the grain boundary by bubbles when saturation occurs. Swelling on the grain face saturates at a value of $f_b \approx 0.25$ [5].

Fig. 1 shows the calculated bubble diameter vs. fission density for three values of grain size. The nominal values of key parameters used in the calculation of Fig. 1 are listed in Table 1. The severity of irradiation-induced re-solution of gas atoms from the boundary to the matrix on intergranular bubble growth is dependent on the ratio λ/d_g: smaller values of λ/d_g lead to larger values for the flux J. As shown in Fig. 1, the calculated intergranular bubble sizes are larger for larger grain diameters (i.e. smaller values of λ/d_g). The arrow in Fig. 1 shows the point at which the grain-boundary bubbles interlink as given by Eq. (22). The effect of calculated grain-boundary bubble diameter on the value of λ/d_g for

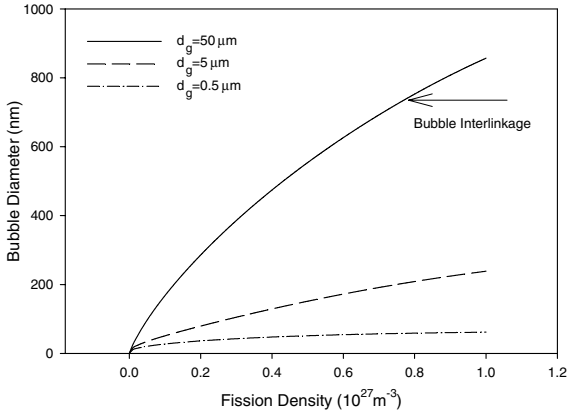

Fig. 1. Calculated bubble diameter vs. fission density for three values of grain size. The arrow shows the point at which the grain-boundary bubbles interlink.

Table 1
Nominal values of key parameters used in the calculation

Parameter	Value	Reference
D_{g_*}	2×10^{-19} m^2/s	[18]
$b_0 f$	2×10^{-4} s^{-1}	[19]
λ	5×10^{-8} m	[15]
N_b	1×10^{12} m^{-2}	[20]
z	10	This work
d_g	5×10^{-6} m	
T	373 K	

a fixed grain size and variable λ is demonstrated in Fig. 2 where calculated bubble diameter vs. fission density is shown for three values of gas-atom knock out distance. Decreasing the value of λ (i.e. smaller values of λ/d_g) leads to larger fluxes and a commensurate increase in the calculated bubble size.

Fig. 3 shows calculated bubble diameter vs. fission density for three values of gas-atom diffusivity. Higher gas-atom diffusion rates result in a greater flux of gas atoms to the boundary (see, Eqs. (13) and (14)) and, thus, larger bubble sizes (a la Eqs. (15) and (16)).

Fig. 4 shows calculated bubble diameter vs. fission density for three values of gas-atom re-solution rate. The re-solution rate that is being varied here is $b_0\overset{*}{f}$, i.e. the term in Eq. (18) that is independent of bubble size. The strength of the gas-atom re-solution rate works counter to that of the gas-atom diffusivity; larger values of the gas-atom re-solution result in a smaller net flux of gas atoms to the boundary (see Eq. (16)) and, hence, smaller grain-boundary boundary bubble sizes. The arrow in Fig. 4 shows the point at which the grain-boundary bubbles interlink. The effect of the back flux of gas atoms can also be seen in Fig. 5, which shows the calculated fractional gas release to grain boundary vs. fission density for three values of gas-atom re-solution rate. For re-solution rates in Fig. 5 of 2×10^{-4} and 2×10^{-3} s^{-1} the fractional gas release decreases after an initial increase. This behavior is due to the growing strength of the back flux of gas atoms as the number of gas atoms in boundary bubbles increases (e.g., see last term in Eq. (16)).

Fig. 6 shows the calculated gas-atom concentration vs. fractional grain diameter across the outer annulus of width λ at a fission density of 1×10^{27} m^{-3} for three values of gas-atom re-solution rate. Higher values of gas-atom re-solution rate result in a stronger back flux of gas atoms into the lattice, and thus a larger concentration of

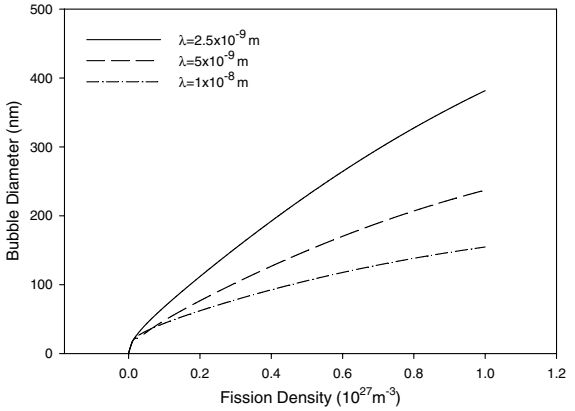

Fig. 2. Calculated bubble diameter vs. fission density for three values of gas-atom knock out distance.

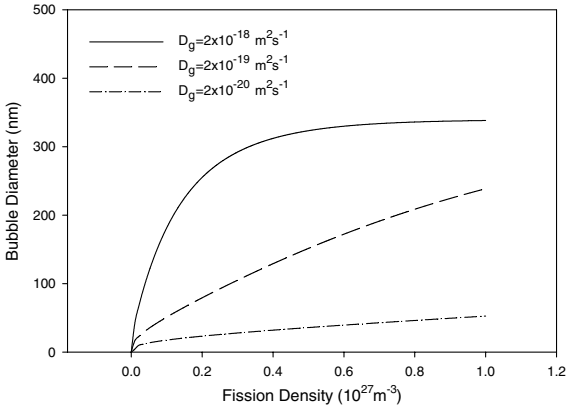

Fig. 3. Calculated bubble diameter vs. fission density for three values of gas-atom diffusivity.

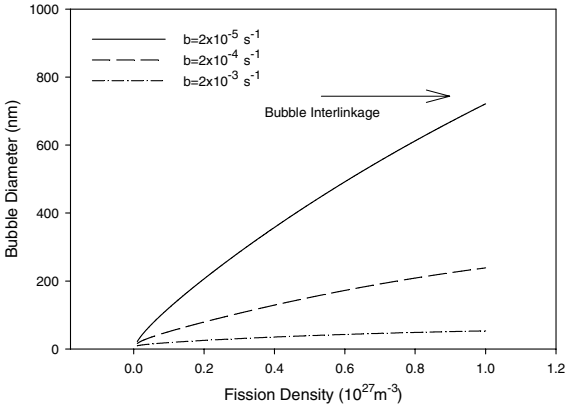

Fig. 4. Calculated bubble diameter vs. fission density for three values of gas-atom re-solution rate. The arrow shows the point at which the grain-boundary bubbles interlink.

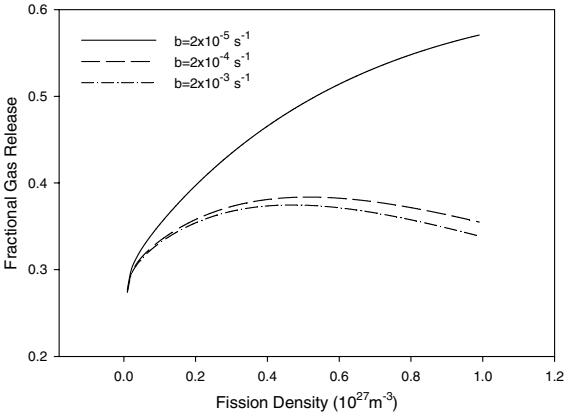

Fig. 5. Calculated fractional gas release to grain boundary vs. fission density for three values of gas-atom re-solution rate.

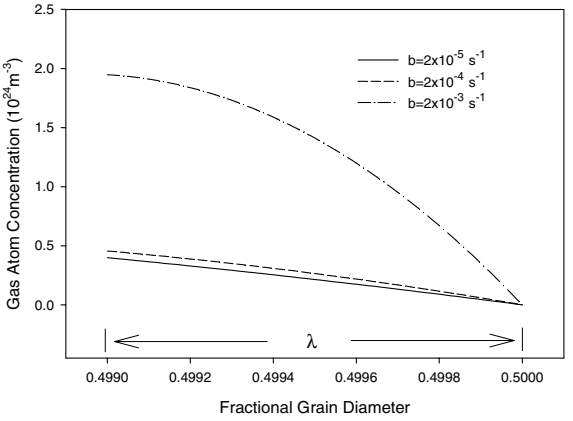

Fig. 6. Calculated gas-atom concentration vs. fractional grain diameter across the outer annulus of width λ at a fission density of 1×10^{27} m^{-3} for three values of gas-atom re-solution rate.

gas within the adjacent annulus of width λ. Although Fig. 6 indicates that the flux of gas to the boundary increases for larger values of the gas-atom re-solution rate, the net flux decreases due to the larger back flux of gas into the lattice. This is clear from Fig. 7 which shows the calculated net flux of gas atoms to the grain boundary vs. fission density for the three values of the gas-atom re-solution rate.

Fig. 8 shows the calculated bubble diameter vs. fission density for three values of grain-boundary diffusion enhancement factor. As expected, larger values of grain-boundary gas-atom diffusivity lead to larger boundary bubble sizes due to the increased flux of gas atoms into the bubbles. The estimated value of the effective intragranular diffusion coefficient given by Eq. (1b) that accounts for gas-atom trapping by intragranular bubbles is well within the range of diffusivities explored in Fig. 8.

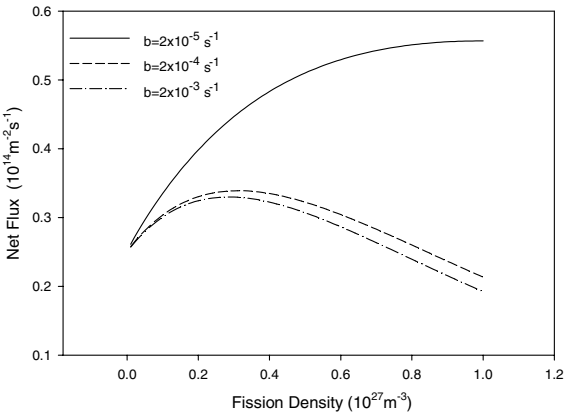

Fig. 7. Calculated net flux of gas atoms to the grain boundary vs. fission density for three values of the gas-atom re-solution rate.

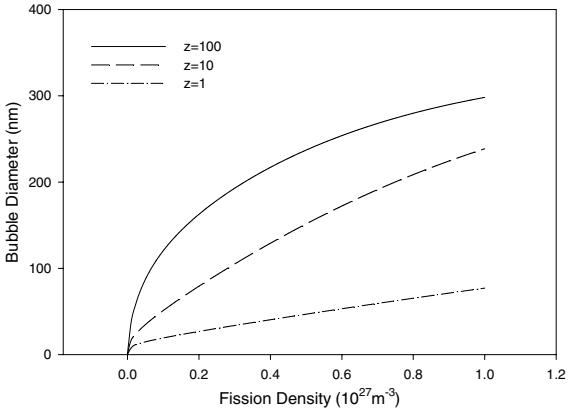

Fig. 8. Calculated bubble diameter vs. fission density for three values of grain-boundary diffusion enhancement factor.

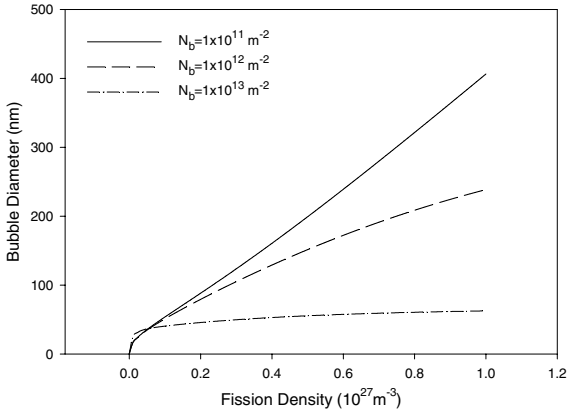

Fig. 9. Calculated bubble diameter vs. fission density for three values of grain-boundary bubble density.

Fig. 9 shows the calculated bubble diameter vs. fission density for three values of grain-boundary bubble density. The calculated bubble size increases for smaller values of the grain-boundary bubble density due to the larger number of gas atoms per bubble.

The temperature used in Figs. 1–9 is 373 K. This low temperature was selected in order to be fully in the athermal, irradiation-enhanced regime. An increase in the temperature (e.g., to 746 K characteristic of the rim region in UO_2 fuel) will, according to Eq. (15), produce a proportionate increase (e.g., doubling) of the bubble diameter.

5. Discussion and conclusions

The effect of irradiation-induced re-solution on the growth of grain-boundary bubbles is not negligible. However, in contrast to bubbles formed in the bulk

material most intergranular bubbles are able to grow to appreciable sizes (i.e. to sizes where grain-face saturation is initiated) due to the following factors. Firstly, with the exception of grains that have extremely high values of boundary area per unit volume (e.g., sub-micron size grains), the flux of gas atoms in a concentration gradient from the matrix to the boundary provide a growth mechanism (i.e. high concentrations of gas and enhanced diffusion) that is much stronger than the bubble growth mechanism in the lattice. Secondly, given the relatively small size of the gas-atom knock out distance λ, gas atoms that are ejected from boundary bubbles find their way back (via the chemical potential gradient) to the boundary in relatively short times. Thirdly, bubble nucleation [21] and growth, linkup, venting, and reformation processes [4,22] on grain boundaries results in bubble densities that are far smaller than observed in the bulk material. For example, an intergranular bubble density of 1×10^{13} m^{-2} is equivalent to a bubble density of 2×10^{18} m^{-3} for a grain size of 5×10^{-6} m. This is to be compared to observe intragranular bubble densities that are on the order of 10^{23} m^{-3}.

The reason for the smaller density of bubbles on the grain boundary as compared to the bulk is also due to the relatively rapid arrival rate of gas atoms to a grain boundary that has substantially smaller volume than the bulk grain. Thus, early in the irradiation the gas-atom interaction rate on the boundary is relatively high leading to an initial rapid nucleation of gas bubbles [3]. These evolving gas bubbles act as sinks for the newly arriving gas and deplete the boundary of single gas atoms thus reducing bubble nucleation. When the projected area coverage of the boundary by bubbles becomes significant, the direct getting of gas atoms arriving from the lattice by the boundary bubbles augments this process. Conversely, within the matrix, although the bubble nucleation rate is initially smaller than on the boundary, the nucleation continues for a longer time leading to a substantially larger, albeit significantly smaller sized population of bubbles [23].

The analysis presented in this paper lacks a calculation for the evolution of the intergranular bubble-size distribution. Instead, the intergranular bubble density is an input parameter (see Table 1). In order to calculate the intergranular bubble density a suitable model for bubble nucleation on grain boundaries is required (such as that developed by Wood and Kear [21]). In the model presented in Ref. [21], the intergranular bubble density rises to a steady-state value relatively early in the irradiation. Although such a calculation is valuable, it was felt that its incorporation was outside of the scope of the present work and would not affect the general conclusions iterated above. However, given an estimate of the intergranular bubble density (e.g., at low burnup) the condition for grain face saturation (i.e. the burnup at which saturation occurs, e.g., see Figs. 1 and 4) can be calculated and compared directly with observation.

Appendix A

The various q coefficients used in Eqs. (8)–(12) are integrals which when evaluated are given by

$$q_1 = 2^9\rho/45,$$

$$q_2 = 2^{10}\rho^3/945,$$

$$q_3 = -q_1,$$

$$q_4 = 2^6\rho^3/189,$$

$$q_5 = q_1 + \frac{4}{(2\rho-1)^4}\left[16/5 - 2^9\rho^5/5 + (2\rho+3)\times\left(2^5\rho^4 + (2\rho+3)(1-8\rho^3)/3 - 2\right)\right],$$

$$q_6 = 856\rho^3/945 + \frac{1}{(2\rho-1)^4}\Big(4(1-(2\rho)^7)/7 + 2(2\rho+3)((2\rho)^6-1)/3 + 4(2\rho+1)\times(1-(2\rho)^5)/5 + (2\rho+1)(2\rho+3)((2\rho)^4-1)/2 + (2\rho+3)^2(1-(2\rho)^5)/5 + (2\rho+1)^2\times(1-(2\rho)^3)/3\Big),$$

$$q_7 = \frac{16}{(2\rho-1)^4}\Big(8((2\rho)^5-1)/5 + (1-(2\rho)^4)(3\rho+5/2) + (2\rho+1)(2\rho+3)((2\rho)^3-1)/3\Big),$$

$$q_8 = \frac{1}{(2\rho-1)^4}\Big(8((2\rho)^7-1)/7 + 2(1-(2\rho)^6)(6\rho+5)/3 + 8((2\rho)^5-1)(2\rho^2+7\rho+2)/5 + (1-(2\rho)^4)\times\left(8\rho^2+10\rho+1\right) + 8\rho(2\rho+1)((2\rho)^3-1)/3\Big),$$

$$q_9 = \frac{64}{(2\rho-1)^4}\Big(4(1-(2\rho)^5)/5 + (2\rho+1)\times((2\rho)^4 + (2\rho+1)(1-(2\rho)^3)/3 - 1)\Big),$$

$$q_{10} = \frac{16}{(2\rho-1)^4}\Big((1-(2\rho)^7)/7 - 2(2\rho)^6/5 - (2\rho)^5/3 + (2\rho+1)^2(1-(2\rho)^5)/5 + (2\rho+1)((2\rho)^6/3 + (2\rho)^5/2 - \rho - 1/3) + 4\rho^2/3 + 4\rho/5\Big),$$

$$q_{11} = 2^6\rho^3/45,$$

$$q_{12} = \frac{56}{45}\rho^3 + \frac{1}{(2\rho-1)^2}\Big(2(1-(2\rho)^5)/5 + (2\rho+3) \times ((2\rho)^4 - 1)/4 - (2\rho+1)((2\rho)^3 - 1)/3\Big),$$

$$q_{13} = \frac{1}{(2\rho-1)^2}\Big(4((2\rho)^5 - 1)/5 + (2\rho+1)(1-(2\rho)^4) + 8\rho((2\rho)^3 - 1)/3\Big).$$

References

[1] C. Baker, J. Nucl. Mater. 66 (1977) 283.
[2] J.A. Turnbull, J. Nucl. Mater. 38 (1971) 203.
[3] M.H. Wood, J. Nucl. Mater. 82 (1979) 264.
[4] J.A. Turnbull, C.A. Friskney, J. Nucl. Mater. 71 (1978) 238.
[5] R.J. White, M.O. Tucker, J. Nucl. Mater. 118 (1983) 1.
[6] D.M. Dowling, R.J. White, M.O. Tucker, J. Nucl. Mater. 110 (1982) 37.
[7] A.D. Brailsford, AERE Report No. R 7446, 1973.
[8] A.J. Manley, TRG Report No. 1681, 1968.
[9] J. Rest, J. Nucl. Mater. 120 (1984) 195.
[10] J. Rest, J. Nucl. Mater. 207 (1993) 192.
[11] J. Rest, G.L. Hofman, J. Nucl. Mater. 231 (2000) 231.
[12] M.V. Speight, Nucl. Sci. Eng. 37 (1969) 180.
[13] J. Spino, D. Baron, M. Coquerelle, A.D. Stalios, J. Nucl. Mater. 256 (1998) 189.
[14] J.R. Matthews, M.H. Wood, Nucl. Eng. Des. 56 (1980) 439.
[15] D.R. Olander, Fundamental Aspects of Nuclear Reactor Fuel Elements TID-26711-PI-ERDA, 1976.
[16] H.J. Hedger, AERE Report No. M 3151, 1980.
[17] G.L. Reynolds, W. Beere, P.T. Sawbridge, J. Nucl. Mater. 41 (1971) 112.
[18] Hj. Matzke, Radiat. Eff. 53 (1980) 219.
[19] M.O. Marlowe, A.I. Kaznoff, in: Nuclear Fuel Performance, Proc. Int. Conf. British Nucl. Soc., London, 1973.
[20] J. Spino, K. Vennix, M. Coquerelle, J. Nucl. Mater. 231 (1996) 179.
[21] M.H. Wood, K.L. Kear, J. Nucl. Mater. 118 (1983) 320.
[22] M.O Tucker, Radiat. Eff. 53 (1980) 251.
[23] J. Rest, R.C. Birtcher, J. Nucl. Mater. 168 (1989) 312.